

## Sticky Rouse Model and Molecular Dynamics Simulation for Dual Polymer Networks

Jingyu Shao, Nuofei Jiang, Hongdong Zhang, Yuliang Yang, and Ping Tang\*



Cite This: *Macromolecules* 2022, 55, 535–549



Read Online

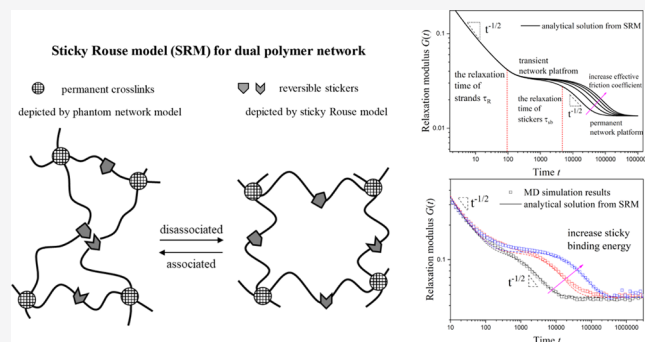
ACCESS |

Metrics & More

Article Recommendations

Supporting Information

**ABSTRACT:** Dual polymer networks with stickers have a reputation for enhanced modulus and toughness. We propose a modified sticky Rouse model (SRM) from the single-chain perspective for permanent and transient dual networks, aiming to find a universal description of associative polymer dynamics. The computational complexity of obtaining the analytical relaxation spectrum is simplified by graph theory, implementing matrix reduction of the Rouse–Zimm matrix based on the symmetry. The analytical relaxation spectrum can also return to the case of linear polymers and permanent networks. The modified SRM for dual polymer networks predicts a Rouse-like scale of the linear relaxation modulus  $G(t) \propto t^{-1/2}$  in sticker relaxation, consistent with the existing experimental results. In particular, the key parameter in the SRM, namely, the effective friction coefficient, can be extracted from the lifetime of sticky bonds and diffusion of chains, obtained by molecular dynamics simulations (MD). Based on that, the SRM model can predict the linear viscoelasticity of dual polymer networks, quantitatively in agreement with our MD results. Our work strongly supports the applicability of the single-chain molecular model SRM for polymer complex networks with reversible associative interactions.



In particular, the key parameter in the SRM, namely, the effective friction coefficient, can be extracted from the lifetime of sticky bonds and diffusion of chains, obtained by molecular dynamics simulations (MD). Based on that, the SRM model can predict the linear viscoelasticity of dual polymer networks, quantitatively in agreement with our MD results. Our work strongly supports the applicability of the single-chain molecular model SRM for polymer complex networks with reversible associative interactions.

### 1. INTRODUCTION

Polymer networks associated with stickers own excellent mechanical properties, exhibiting linear and nonlinear viscoelastic properties, which give them integral roles in many practical scenarios, like tissue engineering, self-healing materials, and shape memory functional materials.<sup>1–3</sup> The excellent mechanical properties come from two contributions, one is the permanent polymer network in a long time scale, and the other is the transient polymer network formed by reversible stickers in a short time scale (seconds to hours in experiments). In particular, the introduction of a small amount of stickers realizes controlling the abundant rheological behaviors of networks through constructing the target structure, where a small change of stickers will raise significant differences in the performance.<sup>4</sup>

Programmable synthesis of new materials with desired mechanical properties is the final goal in polymer science. However, owing to the multiple time scales in dual polymer networks, most of current synthetic strategies can only explore the local optimal structures in a wide parameter space. The limitation of this approach drives significant demand for its theoretical exploration, which completes the knowledge of micro-scale mechanisms rooted in the molecular structures. In most of the literature studies, the Maxwell model is the simplest but most universal phenomenological method for describing the dynamics and rheology of this polymer systems, which combines the spring and dashpot in series.<sup>2,5</sup> In the

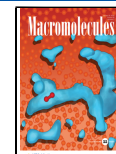
relaxation process of dual polymer networks, the strands dynamics are modeled following Rouse modes, and the relaxation of physical cross-links is estimated as an exponential decay. This can roughly draw out the physical picture of dual polymer network relaxation while ignores the detailed behavior over the whole rheological properties. Recently, Hui and Long et al. developed a constitutive model of dual polymer networks for the stress versus strain response with large strain, which was originally proposed to draw out the breaking of chemically cross-linked double network gels.<sup>3,6,7</sup> The model can present the hysteresis behavior based on the loading and unloading rate, which shows excellent agreement with experiments.

Although many researchers have made profound studies that successfully explain the rheological data observed in experiments, theory adhered to the molecular model like classic Rouse dynamic model has not been claimed. In fact, the pursuit of establishing the concept serving as a molecular model has continued for many years, especially in polymer networks and linear associative polymers.<sup>8,9</sup> In the 1960s,

Received: October 2, 2021

Revised: December 1, 2021

Published: January 6, 2022



Chomppff and Duiser et al. extended the Rouse model to permanent networks and gave a general solution of the relaxation spectrum.<sup>10,11</sup> The series of papers focused on the model with mesh-like networks, which contained numerous local loops. The Rouse model can also describe the polymer network dynamics based on the phantom network, treated as simpler tree-like structures without loops.<sup>12,13</sup> Graessley developed a comprehensive treatment of tree-like Gaussian networks and applied it for the calculation of linear viscoelastic behavior. The analytical relaxation spectrum and modulus were obtained without considering the contribution of strands, namely, the length of strands  $N_s = 0$ .<sup>14–16</sup> Kloczkowski et al. extended Graessley's work to the more realistic case, where a broad relaxation spectrum for molecular internal dynamics and more realistic description were obtained.<sup>17–19</sup> Recently in our work for linear associative polymers, the framework of the sticky Rouse model (SRM) is derived and further verified through molecular dynamics (MD) simulation.<sup>20,21</sup> The rheological properties like linear relaxation modulus were predicted without fitting parameters and showed a quantitative agreement with MD simulations. However, the complex structure of dual polymer networks brings difficulties in modeling and computing costs in simulations. To the best of our knowledge, none have been able to construct a molecular model for predicting the dynamics of dual polymer networks, which acts as a direct liaison between microstructure and macroscopic properties in various practical applications. The permanent and transient dual polymer networks can serve as a model system establishing a universal molecular model for predicting viscoelasticity of sticky polymers. The linear viscoelastic behavior is predicted based on the SRM and phantom Gaussian networks; simultaneously, the affine network model is also used for comparison. The MD simulation is conducted to verify the theoretical results.

This paper is organized as follows: in Section 2, we give the physical picture of dual polymer networks and review the molecular model for sticky polymers and networks. Based on graph theory, the deduction framework of eigenvalue solution of the Rouse-Zimm (RZ) matrix in the SRM model is issued for the relaxation spectrum,<sup>22–24</sup> and the criteria in MD simulation method is discussed. In Section 3, the static and dynamic properties for polymer networks without stickers are discussed based on the numerical solution and MD simulations. In Section 4, the comparison between the analytical and numerical solutions of the Langevin dynamic equation of SRM is presented in the first place. Then, the dynamics properties are studied systematically, establishing the relationship between the structure and performance. A Rouse-like scale of linear relaxation modulus  $G(t) \propto t^{-1/2}$  in sticker relaxation is revealed, and two prediction methods are provided in a parameter-free style. Finally, the conclusions are summarized in Section 5.

## 2. MODEL AND THEORY

The dual polymer network is composed of permanent and transient networks. The transient network formed by the introduction of stickers into the polymer chain and its dynamics can be described by our previously proposed modified single-chain SRM.<sup>20</sup> The modified SRM is also used to predict the dynamic behaviors of the permanent network by considering the structure within the framework of affine and phantom network models. We will describe how the modified SRM is combined with the affine or phantom

network model to investigate the dynamics of dual polymer networks.

**2.1. Dual Polymer Network Model.** The transient network formed by stickers fits in the modified SRM, which describes the sticky segments with distinct effective friction coefficients and verified by MD simulations in our previous work.<sup>20,21</sup> Specifically in our model, the micelles formed by stickers can be simply modeled as suffering a drag force from the background, like a "sticky bead," which has higher effective friction coefficients than the normal beads, as shown in Figure 1.

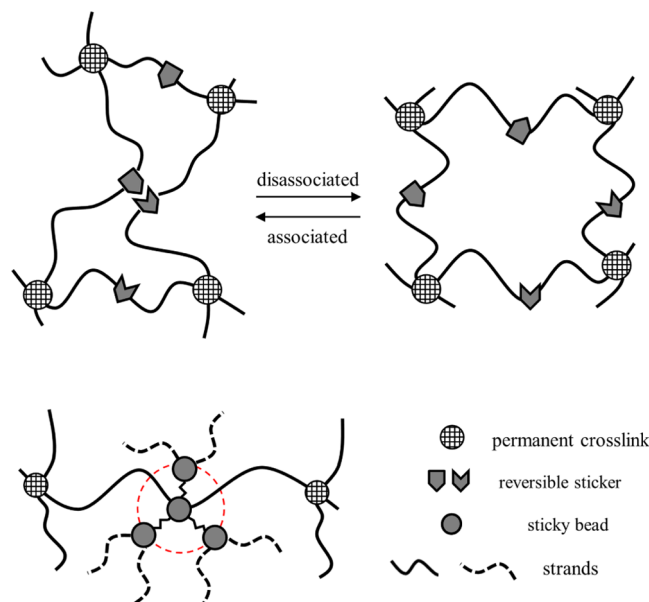


**Figure 1.** Top: Schematic description for the dual polymer network chain model, with only one sticker in the middle of each strand for calculation simplicity. Bottom: The micelles formed by sticker associations feel a drag force from the background imposed by other sticker associations, just like a "sticky bead" with the higher friction coefficient.

Numerous models for the molecular description of polymer networks have been developed, which generally regard the elasticity of the polymer network as entropy elasticity and consider the highly coiled molecular chain as entropy spring.<sup>14–16</sup> The simplest model that captures the characteristic of rubber elasticity is the affine network model proposed by Kuhn, Wall, and Flory et al.<sup>25,26</sup> It is essentially a single-chain model, assuming that the cross-links are fixed in the space and deform affinely with the whole network. However, in polymer networks, each cross-link is attached to other strands, which can fluctuate around the equilibrium position. These fluctuations can reduce the cumulative stretching of the molecular chain and thus decreasing the overall free energy. One of the earliest models that incorporates the fluctuations was developed by James and Guth in the 1940s, known as the phantom network model.<sup>27,28</sup> It considers that the cross-links between strands are free to move, and the macroscopic deformation transmits to the network bulk through the peripheral strands attached to the fixed surface. The Rouse model commonly for the linear polymer chain can be straightforwardly extended to the case of the phantom network by mapping the polymer network structure to a special matrix representing the network topology, like the work of Graessley

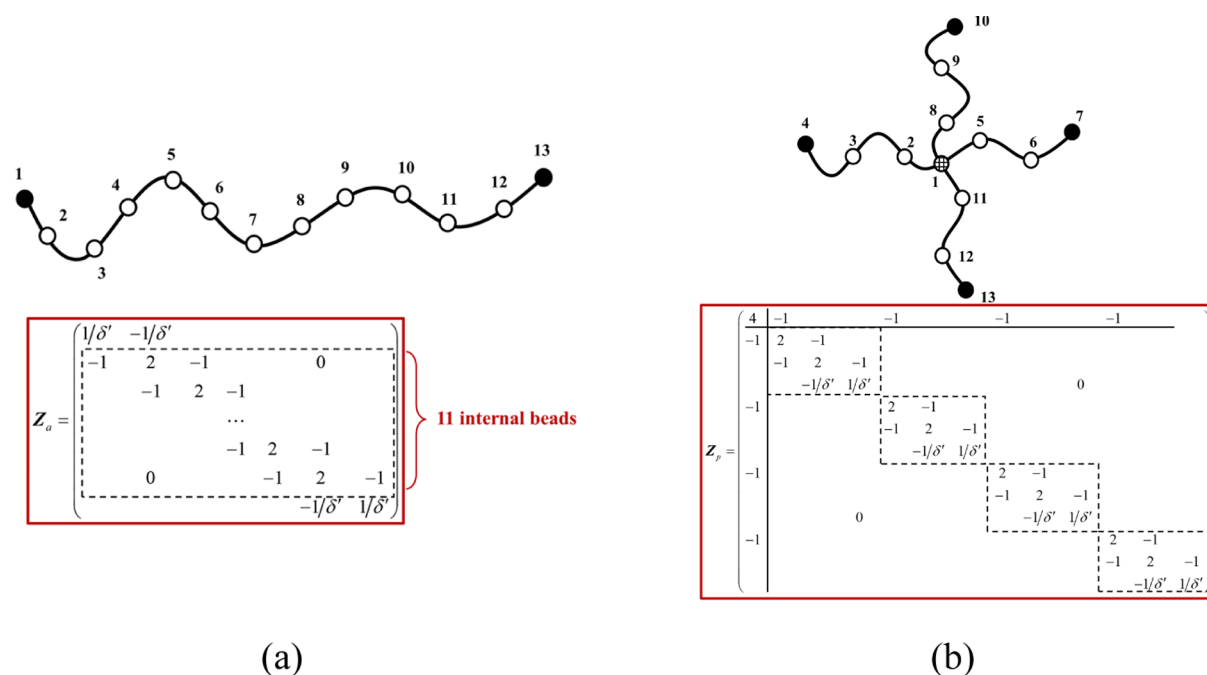


**Figure 2.** (a) Linear structure in the affine network model with its corresponding sticky RZ matrix and (b) tree-like structure in the phantom network with its sticky RZ matrix, both of which have the same segment density.

and Kloczkowski.<sup>14–19</sup> However, this matrix is unlimited extension, and the equilibrium modulus can only be calculated within the classical rubber elasticity theory. In this work, we first introduce the modified SRM into the polymer phantom network model, where the peripheral segments arched in the space are described as the beads with infinite effective friction coefficients.<sup>20</sup>

By introducing stickers on the above permanent polymer networks, the dual polymer network can be constructed, as shown in Figure 1 (for clarity, we only show the local network structure here). We only consider the case with one sticker in the middle of each strand for simplifying the calculation due to too many variable parameters for the dual networks. Although simplified, this complex dual network structure still plays a representative role in understanding the physical pictures of its dynamic motion. All analytical eigenvalues of the Rouse-Zimm (RZ) matrix can be obtained through graph theory, and thus, corresponding linear viscoelastic properties can be presented. With the increased functional groups of cross-links, the results from the phantom network approach to that from the affine network.

**2.2. Modified SRM from a Single-Chain Perspective for Associative Polymers.** The idea of SRM is mainly used to study the linear stress relaxation of associative polymers, which can be traced back to the work of Green and Tobolsky in 1946.<sup>29</sup> Usually, the relaxation time of stickers is much larger than that of strands, and the linear relaxation modulus can be divided into two parts in the limit case. One is the fast relaxation mode of the strands, and the other is the slow relaxation mode of stickers. Chen et al. applied the SRM into ionomers, showing a perfect consistency with the key parameter, namely, association lifetime determined by the dielectric relaxation spectroscopic responses.<sup>30</sup> However, this SRM is based on the phenomenological descriptions, which is not easy to bridge the molecular structure with the final dynamical properties.

To construct the molecular model for predicting the rheological data observed in experiments, we proposed a modified SRM by introducing the concept of the effective friction coefficient, and thus, the mechanical relaxation can be understood from a single-chain perspective. Here, we only give a brief introduction, and the details refer to our previous paper.<sup>20</sup> The calculation method is similar to that of the Rouse model, but we need to modify the Langevin equation of the Gaussian chain modeled as a bead-spring model as follows:

$$\frac{\partial}{\partial t} \mathbf{R}(i, t) = -\frac{3k_B T}{\zeta b^2} \boldsymbol{\Xi}^{-1} \mathbf{Z} \mathbf{R}(i, t) + \mathbf{F}(i, t) \quad (1)$$

with the boundary condition  $\left. \frac{\partial \mathbf{R}_n}{\partial n} \right|_{n=0} = 0$  and  $\left. \frac{\partial \mathbf{R}_n}{\partial n} \right|_{n=N} = 0$ , where the friction matrix  $\boldsymbol{\Xi}$  is a diagonal matrix with diagonal elements of  $\delta_i = \zeta_i / \zeta$  ( $i = 1, 2, \dots, N$ ), which reflects the effective friction coefficient of each bead  $i$ .  $\delta_i = 1$  is for normal beads, and higher  $\delta_i$  is for sticky beads representing the larger effective friction.  $\mathbf{F}(i, t)$  describes time-dependent random force acting on each segment of the molecule,  $\mathbf{F}(i, t) = [f_1, f_2, \dots, f_{N-1}, f_N]$ .  $\mathbf{R}(i, t)$  is the column vector reflecting the positions of beads at time  $t$ , and the superscript  $-1$  represents the transpose of the matrix.  $\boldsymbol{\Xi}^{-1} \mathbf{Z}$  is the sticky RZ matrix that reflects both the information of the chain topological structure and the effective friction of segments (beads). The key step to solve the partial differential eq 1 is finding out eigen-polynomial of the sticky RZ matrix  $\boldsymbol{\Xi}^{-1} \mathbf{Z}$  and calculate its eigenvalues  $\lambda_p$ . Given the  $\lambda_p$ , the relaxation time spectrum is thus obtained as  $\tau_p = \xi b^2 / 3k_B T \lambda_p$ . Thus, we can obtain all linear viscoelasticity properties, such as intrinsic viscosity, compliance, relaxation modulus, storage modulus, and loss modulus.<sup>20</sup>

**2.3. Our Modified SRM Combined with the Polymer Permanent Network Model.** In this work, we combine the modified SRM with the affine or phantom network model to describe the dynamic behavior of permanent networks. Molecular bonds are treated as a Gaussian spring, where the

peripheral segments only receive the tension of one spring, while the internal beads, including the strands and cross-links, will be subjected to the tension of multiple springs. The peripheral segments anchored to the fixed space are represented as the sticky bead with the effective friction coefficient  $\delta_i = \delta' = \infty$  according to the modified SRM above, and all other beads still feel the normal frictional resistance. We apply the Langevin dynamic equation to describe the force balance being applied in the dual polymer network model, which is the same as eq 1. Obviously, different network structures have different sticky RZ matrices, while their peripheral beads have the same infinite friction for describing anchor in the space. For example, we consider the linear structure in the affine network and the tree-like structure in the phantom network, as shown in Figure 2, where the black solid beads are anchored with the infinite effective friction coefficient  $\delta' = \infty$ . The sticky RZ matrix  $Z_a$  of the affine network model is the same as the normal linear chain but the peripheral beads fixed in the space. The  $Z_p$  of the phantom network is partitioned into submatrices for clarity and grows toward the right and downward as increased size of the network. These sticky RZ matrices are real symmetric matrices that can be diagonalized, and the solution of dynamical equations is thus reduced to find its eigenvalues.

Obtaining the eigenvalues of the specific matrix through numerical methods seems straightforward and easy. However, for some complex chain topologies like networks or dendrimers, it is not easy to even express the sticky RZ matrix, and the numerical method is not conducive to understand the intrinsic physics, such as scaling relationship, quantitative analysis, and so forth. The pursuit of analytical solutions of RZ matrix eigenvalues is still significant.

**2.4. Graph Theory for Solving Analytical Eigenvalues of the Sticky RZ Matrix.** The specific physical picture applied in our modified SRM for the affine or phantom dual network model is shown in Figure 3. The affine dual network model is

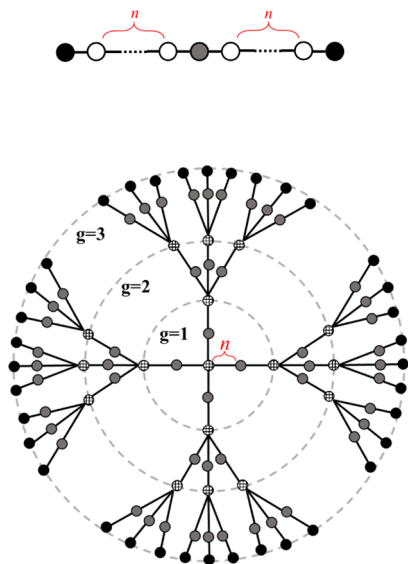


**Figure 3.** Physical pictures of the affine (top) or phantom (bottom) dual network structure. The peripheral segments arched in the space are shown as black solid beads with the infinite effective coefficient, and stickers are gray filled beads located in the middle of strands. The grid bead is the cross-link with functionality of  $\phi$ , and normal segments are not shown out for brevity.

the same as shown in Figure 2a, focusing on the motion of strands with two ends arched in the space, where the only difference exists in the sticky segment. Consistent with the above derivation, the effective friction of peripheral beads (black solid beads, as shown in Figure 3) is assumed as infinity,  $\delta' \rightarrow \infty$ . The extra stickers introduced are shown as gray filled beads, which have a finite but much larger effective friction coefficient than normal beads. The phantom network can be treated as the so-called tree-like structure. For ease of calculation, we adopt dendrimers with well-defined topological symmetry, thus following parameters in dendrimer studies for our model, for example  $\phi$  for the functional degree of cross-links and  $g$  for the generation of dendrimer structures. Figure 3 shows the example with  $g = 3$  and  $\phi = 4$ , and the model approaches network structures with increased  $g$ . In the phantom network model, only the peripheral segments are attached to the surface and deform affinely with the macroscopic deformation. Each grid bead represents a cross-link with  $\phi$  functionalities, and the beads in strands are not shown, where the chain length of each strand  $N_s = 2n + 1$ , and  $n$  is the half strand length.

For slightly complex topologies, like branch or star chain, Zimm and Kilb achieved to diagonalize the RZ matrix through the continuum approximation. Although a certain extent error exists in the assumption, the analytical solution is still a major improvement.<sup>31</sup> Cai and Chen got the exact eigen-polynomials by solving the characteristic equation with the length of strands  $N_s = 0$ . However, the analytical solution only exists in quite simple topologies with low generations  $g$ , and the eigenvalues were only obtained numerically for complex structures.<sup>32</sup> Graph theory was developed by Yang et al. to deal with various complex chain topological structures, which can simplify the RZ matrix using the matrix reduction method by taking advantage of symmetry.<sup>22,24</sup> The method avoids the complicated and tedious mathematical derivation and maps the reduction operation to the topological splitting of chain structures with simplicity and universality. They obtained the analytical eigen-polynomials of the RZ matrix for dendrimers by graph theory and gave analytical eigenvalues in special cases. The detailed graph theory method refers to the previous work of Yang et al.<sup>22,24</sup>

According to graph theory, the diagonalization of the sticky RZ matrix for affine and phantom dual networks can be conveniently implemented. Analytical eigenvalues for stickers can reduce to the Rouse form in the limiting case, and the details can be seen in Sections 1 and 2 in the Supporting Information.

**2.5. MD Simulation. Simulation for the Network.** We adopt the Kremer–Grest (KG) bead-spring model for polymer networks, without considering angular potential. The interaction energy between each unbonded monomer is the Lennard-Jones (LJ) potential energy  $U_{\text{LJ}}$ , where cutoff radius  $r_c = 2^{1/6}\sigma_{\text{LJ}}$  and the number density of LJ bead  $\rho = 0.85/\sigma_{\text{LJ}}$ . We express all quantities in units of the LJ bead diameter  $\sigma_{\text{LJ}}$  intermonomer energy  $\epsilon_{\text{LJ}}$ , and the LJ time  $\tau_{\text{LJ}} = \sqrt{m\sigma_{\text{LJ}}^2/\epsilon_{\text{LJ}}}$ . We model the covalent bond between neighbor beads with the finitely extensible nonlinear elastic (FENE) potential

$$U_{\text{FENE}}(r) = -\frac{kR_0^2}{2} \ln \left[ 1 - \left( \frac{r}{R_0} \right)^2 \right] \quad (2)$$

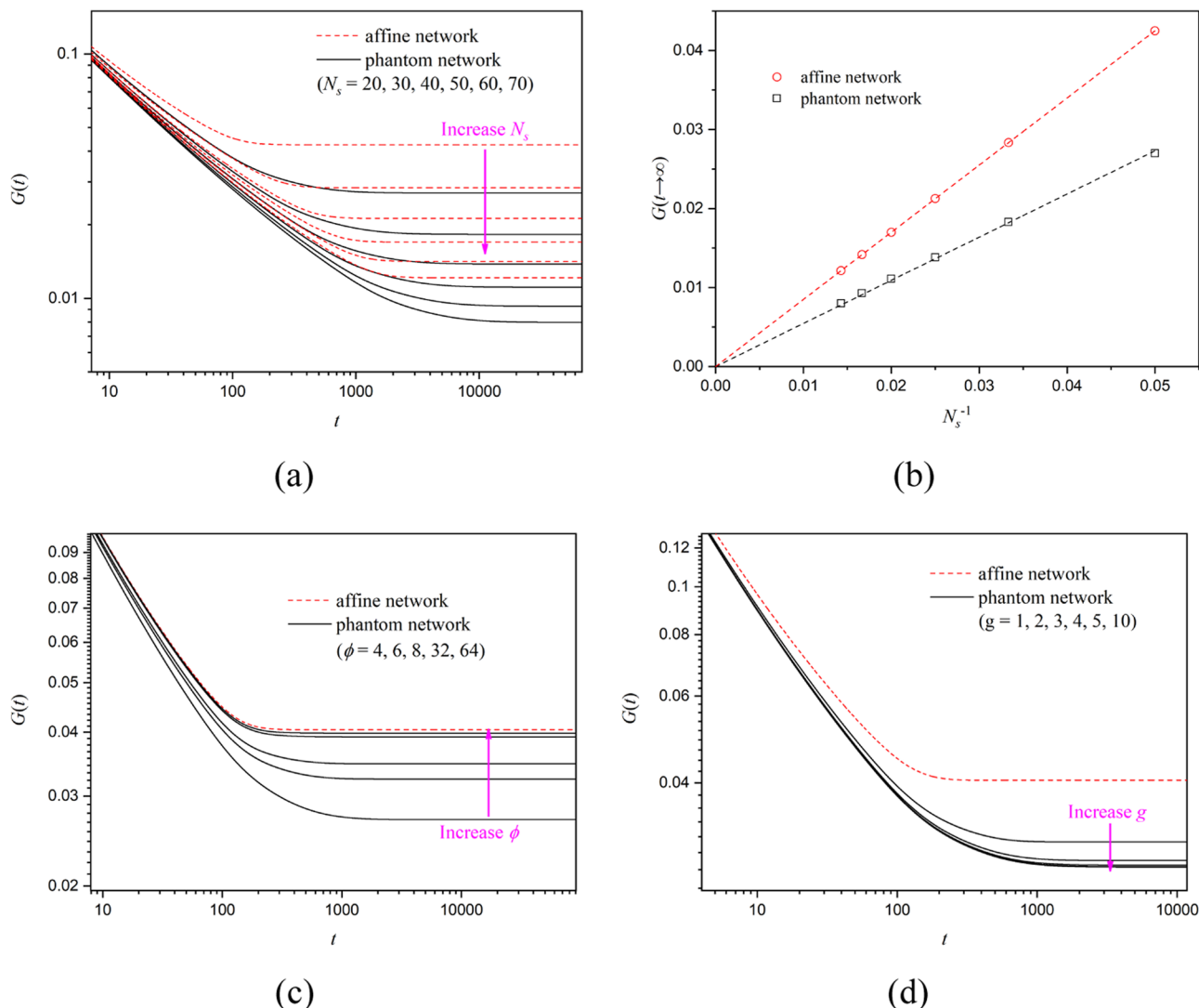


**Figure 4.** Comparison of relaxation modulus  $G(t)$  between phantom and affine dual networks. The influence of (a) strands length, (c) functional degree, and (d) generation in both networks. The results from affine and phantom networks are plotted as red dotted lines and black solid lines, respectively. (b) Equilibrium modulus against the inverse of strand length.

Following most bead-spring studies, we choose  $k = 30\epsilon_{\text{LJ}}/\sigma_{\text{LJ}}^2$  and maximum bond length  $R_0 = 1.5\sigma_{\text{LJ}}$ . All simulations are performed using the LAMMPS with canonical ( $NVT$ ) ensemble under periodic boundary conditions, maintaining the temperature using the Langevin thermostat. Newton's equations of motion are integrated using the velocity Verlet algorithm with a time step of  $\delta t = 0.005\tau_{\text{LJ}}$  at a LJ temperature  $T = 1.0\epsilon_{\text{LJ}}/k_B$ , where  $k_B$  is the Boltzmann constant.

Many problems exist in the end-linked polymer network starting from linear chains, such as spatial inhomogeneities of the cross-link density and the formation of dangling chains and loops, which do not contribute to the network elasticity.<sup>33–35</sup> In our simulation, like divergent synthesizing methods, we directly construct the mesh-like network through end-linking of four-branched star chains (i.e.,  $\phi = 4$  in this work) with each arm length of  $n$ . The first-generation star chain generates randomly like a multifunctional core, and one arm of the second-generation star chain directly grows from one of the end segments of the first generation, avoiding the defect of primary loops. This procedure is then repeated  $M$  times, and the unreacted peripheral beads will undergo the end-linking

during the subsequent relaxation process. The method removes most of the structure defects leaving only a small number of dangling chains, which has few effects on its rheological properties. Fewer defects are helpful to compare our model predictions and simulation results, and we study four networks with  $M \times (4n + 1) = 1500 \times 25, 600 \times 49, 500 \times 69$ , and  $300 \times 101$  beads in this paper. The simulation system applies the periodic boundary conditions.

**Simulation for Stickers.** Sticky monomers have no difference with other LJ beads and are subject to the LJ interaction potential under normal conditions, but they can reversibly break and reconstruct under thermal fluctuations, like hydrogen bonds in real systems. For dual polymer network structures, we introduce a sticker on the middle of each strand, and the two stickers can interact via the potential when they form a reversible sticky bond,<sup>36,37</sup>

$$U_{\text{sb}}(r, h) = U_{\text{FENE}}(r) - U_{\text{FENE}}(r_0) - h \quad (3)$$

where  $r_0 \approx 0.96\sigma_{\text{LJ}}$  is the equilibrium FENE covalent bond length. The sticky binding energy  $h$  is independent of  $r$  and has no contribution to the associative force, which can be written

as  $F_{sb} = -\partial U_{sb}/\partial r$ . However,  $h$  directly relates to the chemical reaction equilibrium without altering the chemical kinetics, namely, it determines the lifetime of sticky bonds. We employ the hybrid MD/MC simulation method to draw the associated and disassociated states of stickers. The formation of a sticky bond between unbonded stickers brings the energy change  $\Delta E(r,h) = U_{sb}(r,h)$  and that for breaking a sticky bond is  $\Delta E(r,h) = -U_{sb}(r,h)$ .<sup>37</sup> At each MC step, the eligible pairs of stickers are chosen first, and then, the attempt of creating a sticky bond is made if the chosen pairs do not reach the maximum saturation and consistent with the setting atom type. However, if the chosen pairs are bonded, the attempt of breaking bonds will be made. The successful probability of each step is the smaller numerical value between 1 and  $\exp[-\Delta E(r,h)/k_B T]$ . We should note that these MC steps are only based on the topology of stickers, which will not change their spatial and velocity distribution. Our simulation is carried out with the small MC time step  $\tau_{MC} = \delta t = 0.005\tau_L$ , which means that MC attempt will be implemented for every MD time step, for reducing the systematic errors in calculating the dynamic properties of dual polymer networks.<sup>37</sup>

Each simulation will experience four equilibration stages. First, the initial network structure is constructed and equilibrated, and this stage lasts multiple Rouse times of the unentangled strand. Second, the unreacted peripheral beads are end-linked, until the unsaturated cross-linkers are within 1%. Then, the simulation system equilibrates multiple of the terminal relaxation time. At last, stickers are introduced and equilibrated, and the stage continues considerably longer due to the much longer relaxation time of stickers. The static and dynamic properties of the reversible network are calculated on the fly over an equilibrium run of the whole polymer dual networks.

### 3. NETWORK PROPERTIES WITHOUT STICKERS

This section considers the static and dynamic properties based on the modified SRM for the permanent network chain without stickers, which served two purposes. First, we choose MD simulation to verify the validity of the single-chain model. Second, our SRM model ignores the chain entanglements, so in this section, suitable chain length parameters for the network without entanglements should be chosen.

The analytical solution of SRM dynamics equation for the network seems to be difficult, while it can be deduced in specific cases. Graessley analytically calculated the stress relaxation modulus through the recurrence formula of the RZ matrix while ignoring the relaxation of strands.<sup>16</sup> Under the same assumption, Yang et al. also calculated the eigenvalues of the RZ matrix for dendritic chains and analytically obtained the similar relaxation spectrum by the graph theory method.<sup>23</sup> As shown in our analytical eigenvalues of eq S.29 in Supporting Information, the eigenvalues can reduce to the same results as in the Graessley and Yang et al. study when  $N_s = 0$  and  $\delta = 1$ ,  $\lambda_{s,k} \approx \left(\phi - 2\sqrt{\phi - 1} \cos\left(\frac{k\pi}{g}\right)\right)/\phi + 2$ , which confirms the reliability of our model from another point of view.

In the framework of the modified SRM for polymer networks, the eigenvalues of the RZ matrix can be directly obtained by the numerical method, and thus, we choose linear relaxation modulus  $G(t)$  to show the overall performance. In the following calculation, we consider the reduced temperature  $k_B T$  and characteristic time  $\zeta b^2/3k_B T$  to be unity, and the

density of segment  $\rho = 0.85$ . The  $G(t)$  is thus simplified as  $G(t) = (\rho/N_s) \sum_{p=1}^{N-1} \exp(-2t\lambda_p)$ , where  $N_s$  is the strand length and  $\lambda_p$  is the eigenvalues with the  $p$  mode. We will discuss the predictions from phantom and affine networks, where the relaxation modulus profiles for different  $N_s$ , generation  $g$ , and functionality  $\phi$  are shown in Figure 4a–d.

Consistent with the previous studies, a permanent rubber network platform appears after strand relaxation, which decreases with the increase in  $N_s$  (increasing  $N_s$  corresponds to decreasing the number density of elastically effective strands), as shown in Figure 4a.<sup>16,35</sup> With the same  $N_s$ , differences between affine and phantom networks become obvious when reaching the permanent network region, where the  $G(t)$  of the affine network remains higher than that of the phantom network. Both equilibrium moduli show  $G(t \rightarrow \infty) \propto N_s^{-1}$ , as indicated in Figure 4b, which is in mutual agreement with the classical rubber network theory. Meanwhile, the scale relationship can be quantitatively obtained in our model. The affine network model, as shown in Figure 2a, has two fixed ends that cannot fluctuate, corresponding to one normal motion mode whose relaxation times tend to be infinite. Based on that, the normalized equilibrium moduli can be directly obtained as  $G_{affine}^{t \rightarrow \infty} \approx \rho/N_s$  when  $t \rightarrow \infty$ , which is the same as the classical rubber network theory. In contrast, for the phantom-based network, the deduction is little tedious and follows the concept of elastically effective strands,  $G_{phantom}^{t \rightarrow \infty} \approx \nu$ , where  $\nu$  is the number density of elastically effective strands after all strands relaxing. The phantom-based network is constructed from the dendrimer structure, and only peripheral fixed segments behave as permanent elastically effective strands. The total segments can be obtained from the recurrence formula.

$$\begin{aligned} N &= N_s[\phi + \phi \times (\phi - 1) + \phi \times (\phi - 1)^2 + \dots \\ &\quad + \phi \times (\phi - 1)^{g_m-1}] \\ &\approx N_s \phi \frac{(\phi - 1)^{g_m}}{\phi - 2} \end{aligned} \quad (4)$$

The number density of permanent elastically effective strands can be directly calculated as,

$$\nu = \frac{\phi \times (\phi - 1)^{g_m-1}}{N} \rho \approx \frac{\phi - 2}{N_s(\phi - 1)} \rho \quad (5)$$

where the scale relationship and the dependence of functionality are analytically obtained. It is clear that the phantom network chain can degenerate to that of the affine network when the functional degree becomes large enough, as shown in Figure 4c and eq 5. The generation  $g_m$  represents the maximum generation in the polymer dual network model, as shown in Figure 3, and larger generation corresponds to more realistic network in qualitative respect. When the generation is small, the relaxation modulus will decrease with increased generation until it reaches to a certain level, where the modulus remains basically unchanged, as shown in Figure 4d. The interesting phenomena of generation influence cannot be explained thoroughly in the current numerical method, which will be further studied analytically in the next section. Different from the results of Graessley et al.,<sup>16</sup> the modified SRM for polymer networks takes into account the local relaxation dynamic of polymer strands and thus can reproduce the fast mode of strands.

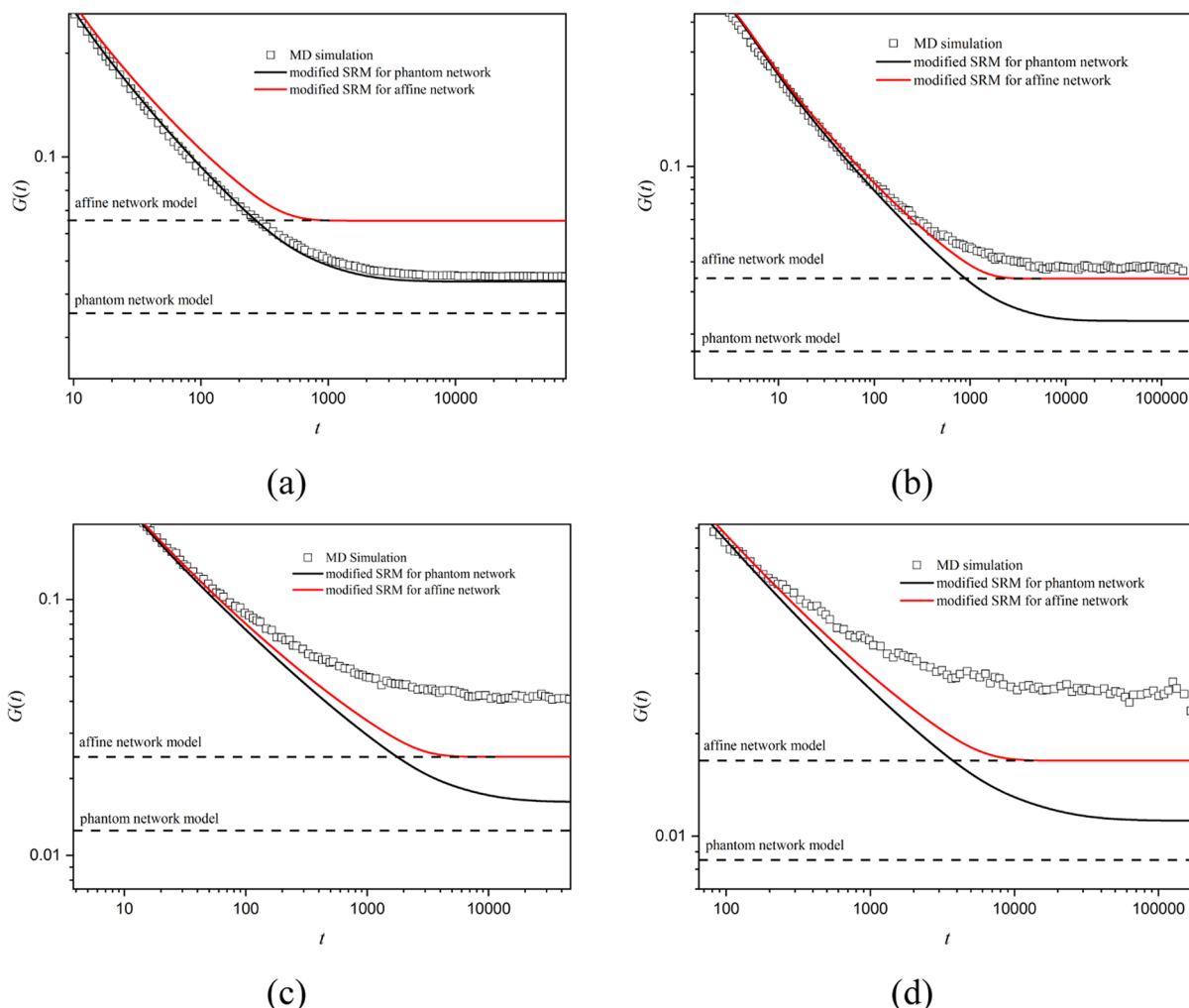


**Figure 5.** Comparison linear relaxation moduli  $G(t)$  between SRM theoretical predictions and MD simulations with (a)  $N_s = 12$ , (b)  $N_s = 24$ , (c)  $N_s = 34$ , and (d)  $N_s = 50$ . The predictions from the modified SRM are expressed as red and black lines, and the predictions from the classical network model are indicated as dashed lines.

MD simulations are further performed for four polymer networks, as depicted in the above section of **MD simulation** with strand lengths  $N_s = 12$ ,  $N_s = 24$ ,  $N_s = 34$ , and  $N_s = 50$ , whose motion of individual junctions is studied (see the **Supporting Information**). As shown in **Figure S4**, strands in networks are Gaussian-like in our simulations, showing  $\langle R^2(N_s) \rangle \propto N_s$  as expected, where  $\langle R^2(N_s) \rangle$  is the mean square end-to-end distance of strands on both the time average and the ensemble average. Besides, the mean square displacement (MSD) of the cross-link in the network with  $N_s = 12$  is in well agreement with the prediction of Erman et al., illustrating that no entanglements exist at this parameter.<sup>17</sup> However, due to the uncrossability of chains, the deviation between them becomes significantly large with increased  $N_s$ .<sup>34,35,38</sup>

In the polymer network, the entanglement mainly comes from the uncrossability of strands, where topological constraints are imposed by the surrounding strands. The modulus is supposed as  $G_N^{t \rightarrow \infty} = \nu k_B T + T_e G_N^0$ <sup>35,38,39</sup> where  $\nu k_B T$  ( $\nu$  is the strand number density) is the rubber elasticity without topological constraints, and  $T_e G_N^0$  is the trapping contribution from entanglements.  $T_e$  is the trapping factor, and  $G_N^0$  is the asymptotic plateau modulus with long enough strands. However, the origins of entanglements for linear chains and polymer networks are essentially different. For

linear counterparts, the critical degree of polymerization (DP) for the entanglement effect has been thoroughly studied,<sup>40</sup> which is supposed to be around 65. The entanglements imposed by neighboring chains restrict their motion, which has a characteristic relaxation time for releasing the topological constraints. For polymer networks, the entanglements root in the formation process for polymer networks, which are permanent trapping at the time when cross-links were formed. In the construction of networks, the reacted ends will retard the motion of the whole chains, and thus that will reduce the critical strand length. According to the work of Grest and Kremer,<sup>35</sup> the  $G_N^{t \rightarrow \infty} \propto N_s^{-1}$  only holds for short chains, which has a deviation at  $N_s = 25\text{--}35$ , that is, the entanglement length in polymer networks.

On the basis of confirming the accuracy of network simulation, we construct each polymer network with six different initial fields, namely formation of six different dendrimers. We calculate the linear viscoelasticity of each dendrimer and then obtain the average results to avoid the sample deviation. Each relaxation moduli  $G(t)$  is obtained through fly calculation of time correlation functions by Likhtman et al.<sup>41</sup> As shown as hollow squares in **Figure 5a-d**, our simulations run up to  $6 \times 10^8$  time steps and are sufficient to reach the plateau regime for the permanent rubber

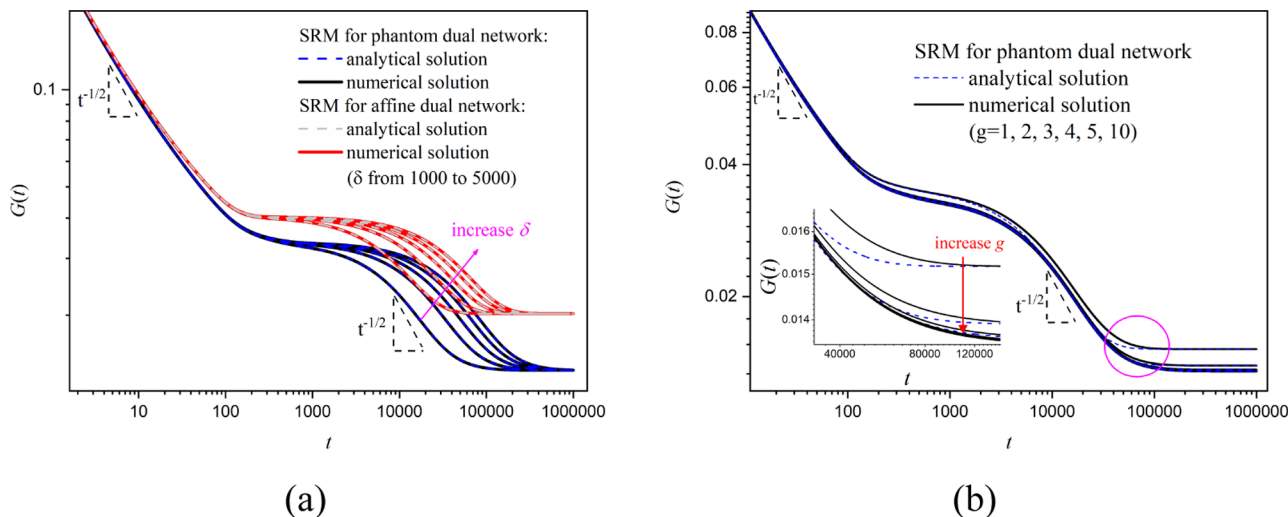


**Figure 6.** Comparison between the  $G(t)$  obtained from analytical and numerical calculations of our modified SRM dual networks under variable (a) effective friction coefficient  $\delta$  and (b) generation  $g$ . The dotted and solid lines represent analytical and numerical solutions of SRM, respectively.

networks. The results conform to the previous conclusion, and we present these findings in Table S1. The background friction coefficient  $\zeta$  is determined by fitting, which is approximately equal to 24 for four simulations, basically unchangeable with invariant number density. The case of Figure 5a with  $N_s = 12$  is consistent with the prediction of the modified SRM for the phantom network. The network in this case has few entanglements and behaves like a perfect network, whose modulus locates between the two classical affine and phantom network theories. Moreover, our MD simulation has a perfect consistent modulus with our modified SRM prediction and deviates from the predicted modulus of the classical phantom network deducted within the assumption of parallel strands. The topological constraints will inevitably increase with increased strands. As a result, the case with  $N_s = 24$ , as shown in Figure 5b, has the modulus that is slightly higher than the predicted value based on the phantom model, but it still locates in a reasonable error range within the affine network framework, where trapping contribution from entanglements is only  $0.003\epsilon/\sigma^3$ . The chain uncrossability limits the motion of cross-links, causing the relaxation of the whole network contributed by that of one strand. With a continuous increase in the strand length, the degree of intertwining between strands will follow up, and the trapping contribution from entanglements  $T_e G_N^0$  becomes notable. For the simulation with  $N_s = 34$  and  $N_s = 50$ , the trapping contributions are  $0.016\epsilon/\sigma^3$  and  $0.009\epsilon/\sigma^3$ , which locate in a range of entanglement chain length from the work of Grest and Kremer, as supposed to be  $0.017\epsilon/\sigma^3$  for the asymptotic plateau modulus  $G_N^0$ .<sup>35</sup> With the obvious entanglements effect, the moduli, as shown in Figure 5c,d, even exceed the prediction of the affine network.

The main purpose in Section 3 focuses on the available single-chain model in the polymer network and suitable parameters for MD simulation. The agreement in Figure 5a shows a perfect applicability of the modified SRM for polymer networks, describing the linear relaxation process within the whole rheological frequency range. We should note again that the entanglement constraints will complicate the stress relaxation mechanism, and this work focuses on the short-chain system  $N_s = 12$  with negligible entanglement effect. With

the analytical solution of relaxation spectrum obtained, the more interesting dynamics can be obtained.

#### 4. DUAL POLYMER NETWORK PROPERTIES

From the modified SRM, we can obtain the analytical eigenvalues of dual polymer networks through graph theory, as shown in the Supporting Information, which can provide the whole relaxation modes, reflecting all microscopic relaxation mechanisms in such polymers. The accuracy is presented first from the linear relaxation modulus  $G(t)$ , as shown in Figure 6a. The setting of reduced temperature, characteristic time, and segment density is the same as mentioned above. Intuitively, we find that the analytical results are in perfect agreement with the numerically solved SRM results, whether obtained from the affine or phantom network. The relaxation time of stickers becomes large with increased  $\delta$ , and the height of the modulus platform remains unchanged, demonstrating that only the time span of the linear relaxation modulus is affected by the association strength of stickers, which is consistent with the results of previous studies in associative polymers.<sup>20,42,43</sup> The  $G(t)$  shows two characteristic relaxation times corresponding to strands and stickers, respectively. Obviously, the dual polymer network first experiences the strand relaxation and reaches a modulus platform at the Rouse relaxation time  $\tau_R$ , that is, the transient network composed by stickers. When the relaxation behavior lasts long enough, stickers begin to diffuse during the association–disassociation process, and the  $G(t)$  deviates from the plateau region, which is the characteristic relaxation time of stickers. Interestingly, a scale of  $G(t) \propto t^{-1/2}$  exists in the relaxation process of the transient network according to our model predictions, which indicates that the sticker relaxation process in dual polymer networks also follows the Rouse relaxation mode, and this has not been carefully studied before. As early as 1989, Baxandall et al. proved that the sticker relaxation behavior in linear chains is consistent with the Rouse relaxation mode using the probability distribution and characteristic time of the sticker reaction.<sup>9</sup> This finding has been widely applied in linear sticky chains, while no existing theory can clarify the sticker relaxation mode on the dual polymer networks, which will establish a unified theoretical framework for all sticky systems. Experimentally, Sheiko et al. constructed master curves of time-average

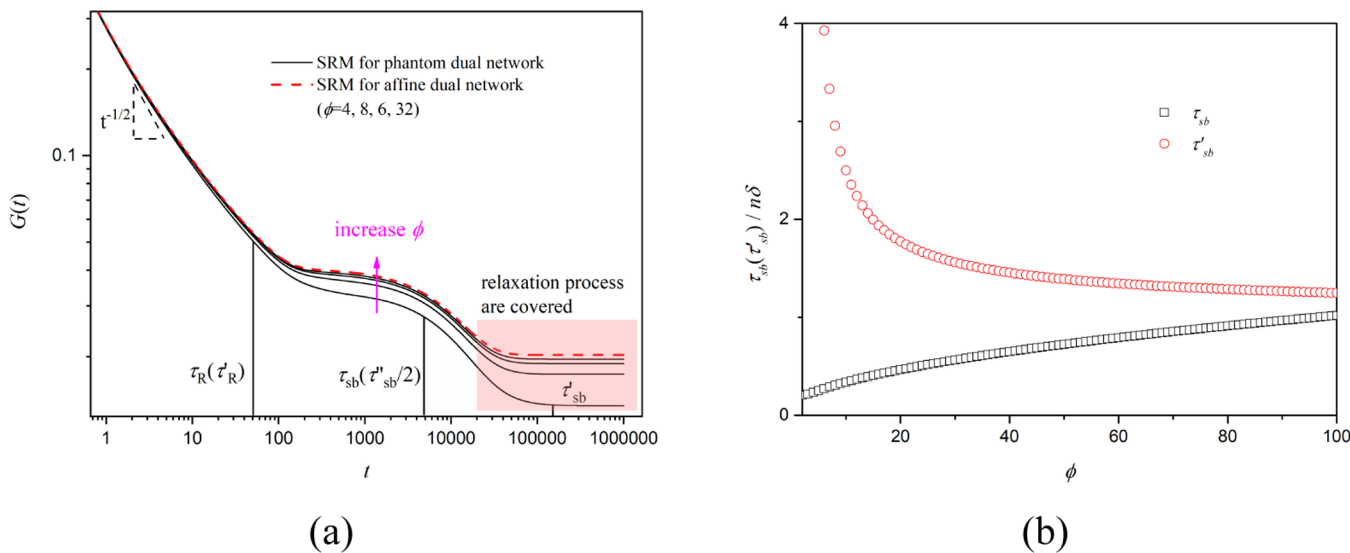


**Figure 7.** When  $n = 20$ ,  $\delta = 1000$ , and  $g = 10$ , changes in (a)  $G(t)$  and (b) its characteristic time with functionality  $\phi$ . Results from affine and phantom networks are presented as red dotted and black solid lines, respectively.

Young's modulus from the stress-strain curves at different strain rates for dual polymer networks,<sup>5</sup> where the temperature ranges from 3 to 37 °C, and all master curves have the  $G(t) \propto t^{-0.5}$  in the time scope between  $10^{-3}$  and  $10^{-2}$  s. However, the scale of  $G(t) \propto t^{-0.5}$  with the temperature higher than 3 °C is no longer caused by the strand motion because of a quick motion at the higher temperature. According to our model prediction and the experiments results, this  $G(t) \propto t^{-0.5}$  in higher temperature case represents the relaxation of stickers followed by exponential decay relaxation, which is also consistent with our findings. It should be noted that the two Rouse relaxations are coupled with transient and permanent networks, respectively, leading to a little deviation on  $G(t) \propto t^{-1/2}$ , as observed in our previous work.<sup>20</sup> Similar to the results of Figures 4d, Figure 6b concludes that a certain deviation between the numerical and analytical results exists when generation  $g$  for the phantom network is small, which becomes negligible with increasing  $g$ .

In this section, we start from the analytical eigenvalues in the modified SRM of the phantom dual polymer network model and explain the reason for the existence of scaling and convergence (with  $g$ ) from the dynamic properties. The overall linear relaxation modulus can be directly calculated from contributions of subgraphs (for details, see the Supporting Information). The analytical eigenvalues are divided into the general solution  $\lambda_p$  of strands and  $\lambda_{s,k}(\lambda_s)$  of stickers, where  $\lambda_s$  is calculated from the sticker in  $P_{(0)B}(x)$  without translational symmetry. Without considering the relaxation of peripheral arched segments, the analytical solution of  $G(t)$  can be drawn out as the function of five different characteristic relaxation times based on the above assumptions. See the Supporting Information for the detailed derivation, where the  $G(\phi,t)$  converges with large generation  $g$ .

$$G(\phi, t) = \frac{1}{2\sqrt{2}} \left( 1 - \frac{(\phi - 2)^2}{(\phi - 1)^2} \right) \left[ \frac{\rho}{2n + 2} \left( \frac{\pi\tau_R}{t} \right)^{1/2} + \left( \frac{\pi\tau_R'}{t} \right)^{1/2} + \left( \frac{\pi\tau_{sb}}{t} \right)^{1/2} \exp\left(-\frac{2t}{\tau'_{sb}}\right) \right] + \frac{(\phi - 2)^2}{(\phi - 1)^2} \frac{\rho}{2n + 2} \left[ \left( \frac{\pi\tau_R}{2t} \right)^{1/2} + \exp\left(-\frac{t}{(\tau''_{sb}/2)}\right) \right] \quad (6)$$

where  $\rho$  is the density of segments. When  $\phi = 2$ , eq 6 can reduce to the linear relaxation modulus of linear chains,

$$G(2, t) = \frac{1}{2\sqrt{2}} \left( \frac{\rho}{2n + 2} \right) \left[ \left( \frac{\pi\tau_R}{t} \right)^{1/2} + \left( \frac{\pi\tau_R'}{t} \right)^{1/2} + \left( \frac{\pi\tau_{sb}}{t} \right)^{1/2} \exp\left(-\frac{2t}{\tau'_{sb}}\right) \right] \approx \frac{1}{2\sqrt{2}} \left( \frac{\rho}{2n + 2} \right) \left[ \left( \frac{\pi\tau_R}{t} \right)^{1/2} + \left( \frac{\pi\tau_{sb}}{t} \right)^{1/2} \exp\left(-\frac{2t}{\tau'_{sb}}\right) \right] \quad (7)$$

which is consistent with the linear relaxation modulus expression of SRM by Chen et al.<sup>30</sup> The  $G(t)$  can be divided into two parts. One is the fast relaxation mode of the strands, and the other is the slow relaxation mode of stickers. So far, the above convergence with  $g$  is described from the dynamical properties of dual networks, whose analytical linear relaxation modulus is directly obtained. Moreover, the scale of  $G(t) \propto t^{-1/2}$  existing in the relaxation process of both strands and stickers, which explains our numerical and analytical results of  $G(t)$ , is shown in Figure 6. The corresponding experiment in the Supporting Information can be found in the master curves of the modulus by Sheiko et al.<sup>5</sup>

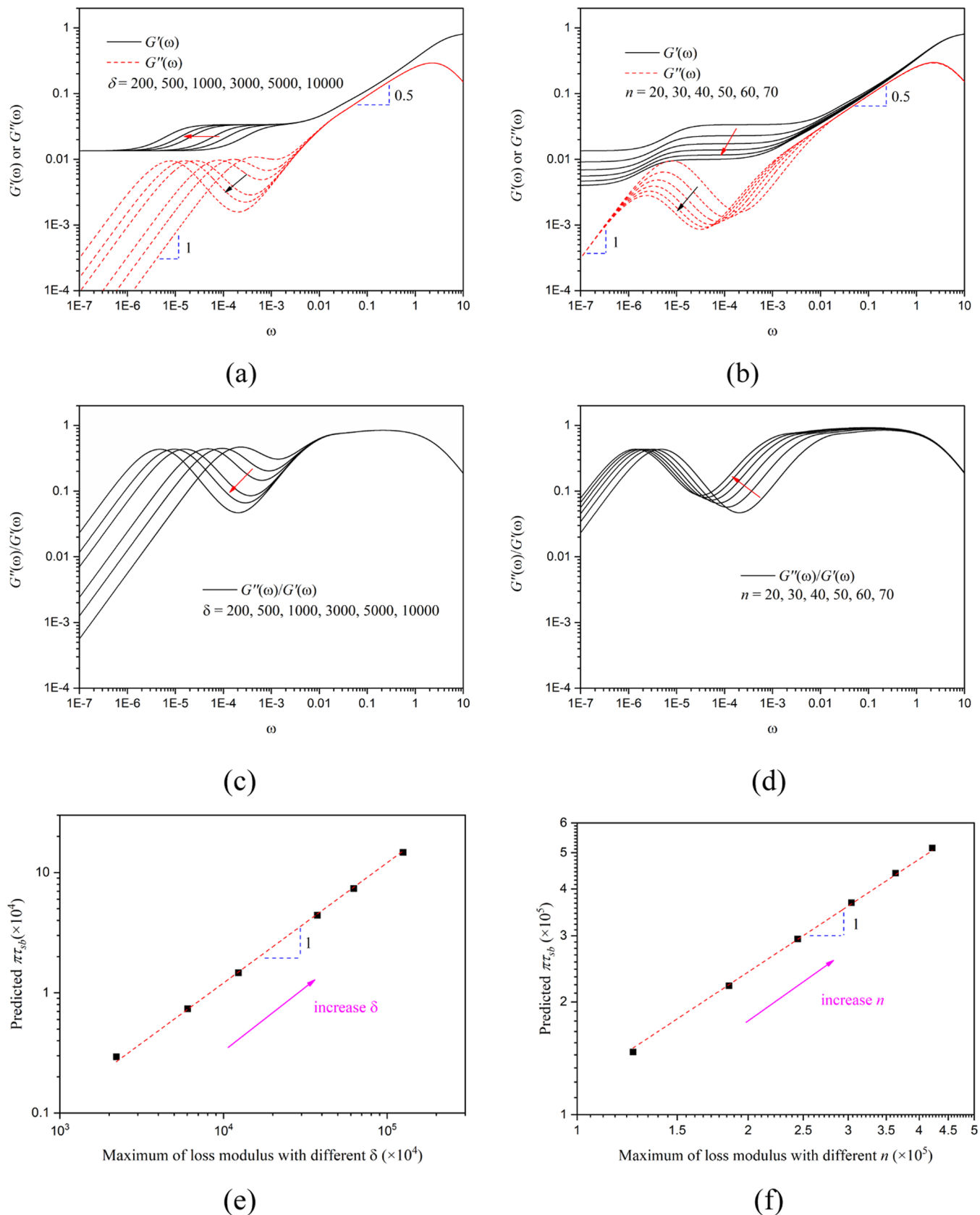


**Figure 8.** Changes in the storage modulus  $G'(\omega)$  and loss modulus  $G''(\omega)$  for dual polymer networks are shown with (a) effective friction coefficient  $\delta$  and (b) half strand length  $n$ . Changes in the loss tangent  $G''(\omega)/G'(\omega)$  with (c)  $\delta$  and (d)  $n$ . Comparison between the characteristic time determined from the maximum of loss modulus and eq 10 under different values of (e) effective friction coefficient  $\delta$  and (f) half strand length  $n$ . Arrows direct the increase in  $\delta$  or  $n$ .

As shown in eq 6, characteristic relaxation times are obtained with the assumption of characteristic time  $\zeta b^2/3k_B T$  to be unity.

$$\tau_R = \frac{(n+1)^2}{\pi^2} \quad (8)$$

$$\tau'_R = \frac{(2n+1)^2}{4\pi^2} \quad (9)$$

where the two strand relaxation times tend to be the same with large  $n$ ,  $\tau_R \approx \tau'_R$ , which represents the relaxation of both half strands separated by stickers, respectively.

$$\tau_{sb} = \frac{\phi n \delta}{\sqrt{\phi - 1} \pi^2} \quad (10)$$

$$\tau'_{sb} = \frac{\phi n \delta}{\phi - 2\sqrt{\phi - 1}} \quad (11)$$

$\tau_{sb}$  and  $\tau'_{sb}$  are the characteristic time and truncation time of stickers, respectively. When the relaxation time far exceeds the characteristic time of stickers  $\tau_{sb}$  and approaches the truncation time  $\tau'_{sb}$ , stickers will relax following the exponential decay. In addition, eq 6 also describes the influence of functionality on the linear relaxation modulus  $G(\phi, t)$ , where the modulus tends to be determined by subgraph B ( $P_{(0)B}(x)$ ) with large functionality. Thus, the fluctuation of cross-links is suppressed, and the phantom network approaches to the affine network during the relaxation, as shown in Figure 7a with  $n = 20$ ,  $\delta = 1000$ , and  $g = 10$ , where the characteristic relaxation times are reduced to  $\tau_R$  and  $\tau''_{sb}$ .

$$\frac{\tau''_{sb}}{2} = \frac{n \delta}{4} \quad (12)$$

However, the characteristic time of stickers  $\tau_{sb}$  are approximately consistent with  $\tau''_{sb}$  accidentally at the chosen parameters. A transition in the scale of the relaxation process also happens with increased  $\phi$ , which changes from Rouse relaxation to an exponential decay during the sticker relaxation drawn out analytically in eq 6, same as the existing experiments.<sup>5</sup> As  $\phi$  becomes larger, the difference between  $\tau_{sb}$  and  $\tau'_{sb}$  is decreasing, which accelerates the transition of scales, that is, the Rouse relaxation mode of stickers will disappear when the functionality reaches a high degree, as shown in Figure 7b. However, it should be noted that the transition of scales is covered in Figure 7a because of the existing permanent networks.

For achieving the target rheological properties by the design of molecular structures, we can further calculate other mechanical properties of dual polymer networks, like the storage modulus  $G'(\omega)$ , loss modulus  $G''(\omega)$ , and stress-strain relations. The results are simplified similar to the method mentioned above, where reduced temperature  $k_B T$  and characteristic time  $\zeta b^2/3k_B T$  are set to be unity, as shown in Figure 8a,b. Furthermore, the changes in the loss tangent  $G''(\omega)/G'(\omega)$  with  $\omega$  are shown in Figure 8c,d for describing the relaxation mode at different parameters. Generally, the storage modulus  $G'(\omega)$  is always greater than the loss modulus, and no intersection between them exists in the full frequency region, indicating the nature of solid elasticity. Two plateau regions of the storage modulus  $G'(\omega)$  occur, one of which locates at the intermediate frequency caused by the transient network, and the other is due to the permanent

network platform at a low frequency. For the loss modulus  $G''(\omega)$ , three transitions exist in the relaxation process. The first transition happens when strands begin to relax from the “frozen” state at a high frequency, where the loss tangent locates at the higher level and then decreases with the transient network dominating. The second transition occurs when stickers begin to disassociate, and the loss modulus reaches a minimum value at this transition point. The third transition locates at the low-frequency region, where the loss modulus and tangent both reach a maximum, and thus, the dual polymer network begins to show the nature of solid elasticity.

We further consider the changes in  $G'(\omega)$  and  $G''(\omega)$  with  $\delta$  and  $n$ . As shown in Figure 8a,c, large  $\delta$  only affects the dynamics of the stickers, which increases both elastic characteristics and relaxation time of stickers with a decrease in the minimum values of loss modulus and tangent. The transient network formed by stickers lasts longer with large  $\delta$ , which contributes to the modulus by increasing the lifetime between stickers. However,  $G'(\omega)$  under all  $\delta$  tend to converge to a constant in the low-frequency region, demonstrating that the permanent network is not affected by  $\delta$ . Compared with the change in  $\delta$ , the influence of  $n$  is slightly complicated, which affects the structure of the permanent network, leading to the non-convergence of  $G'(\omega)$ , as shown in Figure 8b,d. From the perspective of the loss tangent, the minimum value during the intermediate-frequency region decreases with increased  $n$ , indicating more viscous flow characteristics. Although both large  $\delta$  and  $n$  can extend the relaxation of stickers  $\tau_{sb}$ , they have a contrary effect on the dynamical performance (elasticity or viscous characteristics). Moreover, we construct the stress-strain curves of small deformations based on the mechanical properties of  $G(t)$ , measured at different strain rates, where the tensile stress increases with time at a constant strain rate  $\dot{\epsilon}$ :

$$\sigma(t) = \int_0^t G(t-t') d\epsilon(t') = \dot{\epsilon} \int_0^t G(\tau) d\tau \quad (13)$$

Figure S5 shows the stress-strain curves of small deformations with strain rates ranging from  $1.5 \times 10^{-7}$  to  $5 \times 10^{-3} \text{ s}^{-1}$ . The theoretical results agree with the existing experiments in the linear region, where the linear relaxation modulus of the dual polymer network becomes larger with the increased strain rate.<sup>5</sup> This means the dual polymer network can translate from the soft network to the rigid network with the increase in the strain rate.

With the assumption that the characteristic relaxation frequency locates at the maximum of loss modulus, we compare their reciprocals (namely, relaxation time) in different  $\delta$  and  $n$  with the analytical expression of characteristic relaxation time deduced above in eq 10, as shown in Figure 8e,f. The estimated sticker characteristic relaxation time shows a good one-to-one correspondence with our analytical characteristic relaxation time, meaning that the analytical expression (eq 10) can be directly used to estimate the rheological properties of the dual polymer network. To further confirm the conclusion, we further carry out the related MD simulations.

Here, we focus on the predictive power of our modified SRM for the dual polymer network model, offering the supporting results of MD simulations. We propose two ways to obtain the effective friction coefficient  $\delta$  in SRM, by calculations from MD simulations. The specific simulation details, including the parameters and MC process of sticker

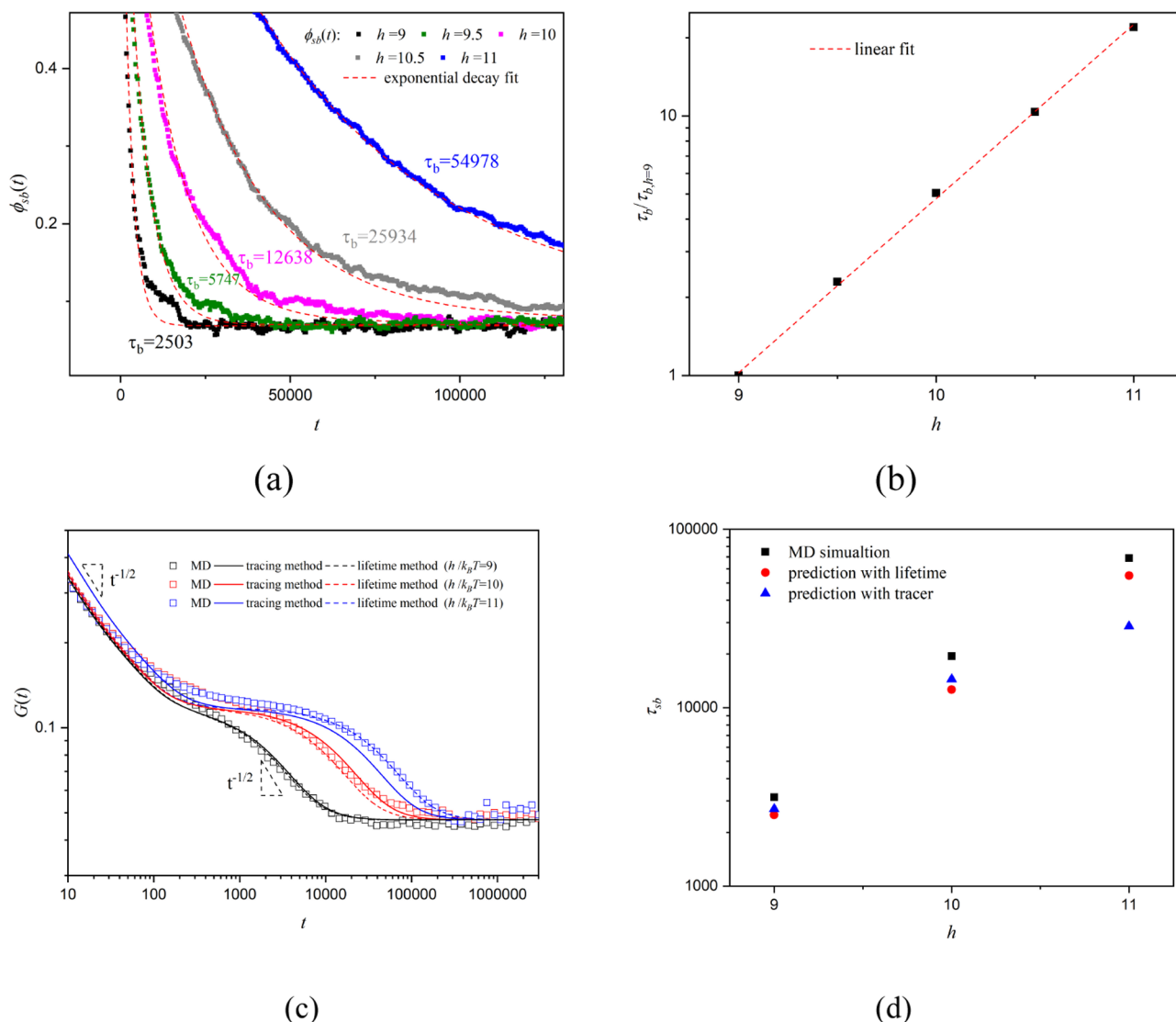


**Figure 9.** Quantitative comparison between predictions and simulation results through two methods. (a) Lifetime before a sticker finds new partners. (b) Arrhenius relationship between the binding energy  $h$  and the bond lifetime  $\tau_b$ . For avoiding the influence of  $\tau_{b,0}$ , we present the ratio between  $\tau_b$  and  $\tau_{b,h=9}$ . (c) Linear relaxation modulus obtained from SRM predictions and MD simulations. (d) Characteristic relaxation times determined from fitting against that from predictions.

simulation, are shown in Section 2.5. Here, we should note the method of our initial field setting. The polymer networks with the half strand length  $n = 6$  are chosen without entanglements, which is proved above. We place stickers with a functionality of 2 in the middle of stands and perform with sticky binding energy  $h$  ranging from 9 to 11, each of which is pre-equilibrium  $1 \times 10^9$  steps and run up to  $2 \times 10^{10}$  time steps for the final equilibrium. Similar to the simulations of the polymer network, we obtain its linear relaxation moduli  $G(t)$  through fly calculation of time correlation functions, as scatters shown in Figure 9c. The overall rheological properties are mutually consistent between the experiments, MD simulations, and analytical solutions of SRM prediction, where the transient network platform modulus appears in the intermediate relaxation time, followed by the chemical network platform as discussed above. The characteristic relaxation time increases with increased  $\delta$ . The scales of  $G(t) \propto t^{-1/2}$  are observed in both relaxation processes of strands and stickers, which

perfectly agrees with our deduction of the phantom dual polymer network model.

For the systems of ionomers or other polymers, the lifetime of stickers  $\tau_b$  can be obtained through characterizations like dielectric spectra. Based on the assumption of the lifetime of stickers  $\tau_b = \pi\tau_{sb}$ , we can find all the parameters needed in the modified SRM for dual polymer networks, namely,  $n$ ,  $\phi$ , and  $\delta$ . Thus, the model can predict the linear relaxation modulus with the characteristic time  $\zeta b^2 / 3k_B T$  obtained from the fitting with experiments or MD.<sup>30</sup> In our MD simulations, the lifetime of stickers  $\tau_b$  can be directly obtained through the bond information by defining the density of sticky bonds alive after time  $t$  as,

$$\phi_{sb}(t) = \frac{n_{sb}(t)}{n_{sb}(0)} \quad (14)$$

where  $n_{sb}(t)$  represents the number of surviving sticky bonds between stickers at time  $t$ , and  $n_{sb}(0)$  is the initial number of bonds. With the sufficiently high bonding energy in our

simulations, the recombine process between the open stickers and their old partners is most likely to occur.<sup>43,44</sup> Therefore, we define the existing time before a sticker finds new partners in its lifetime when considering the breaking and reforming process. Figure 9a shows the curve of  $\phi_{sb}(t)$  against  $t$  by MD simulations, fitted by an exponential decay function  $\phi_{sb}(t) = A \exp(-t/\tau_b)$  in the red-dotted lines, where  $A$  is the prefactor. Figure 9b shows the lifetime of stickers  $\tau_b$  for different values of binding energy, obtained from the fitting  $\phi_{sb}(t)$  against  $t$  by MD simulations. The increase in binding energy  $h$  directly leads to the higher lifetime, which is in agreement with the Arrhenius relationship,

$$\tau_b \approx \tau_{b_0} \exp(h/k_B T) \quad (15)$$

where  $\tau_{b_0}$  reflects the reaction rates of stickers in the hybrid MD/MC simulation. Based on the assumption of  $\tau_b = \pi\tau_{sb}$ , the key parameter  $\delta$  in our model can be directly obtained using eq 10. Specifically, we calculate  $\delta$  as 56.81, 266.37, and 1205.3 for  $h$  from 9 to 11. The prediction is shown as dashed lines in Figure 9c, showing a quantitative consistency. Here, a revision is needed on  $n$ , which seems to be corrected as  $n = 5$ . The essential reason is the partial coupling between the dynamics of backbones and stickers, which brings a reduction in adjacent segment motions, equivalent to a longer Kuhn length of stickers.<sup>30</sup> The next method also follows this revision. The only fitting parameter is the characteristic time of the unit bead  $\zeta b^2 / 3k_B T$ , that is, the background friction coefficient  $\zeta$ . Comparing to that in the simulations of networks, the existing stickers bring the decrease in diffusion capacity, and thus,  $\zeta$  becomes smaller. However, for a basic invariant molecular system, such as the number density and segment types (sticky or non-sticky),  $\zeta$  is basically unchangeable that equals to 37. This invariant feature is also shown in Figure 9c that Rouse relaxation processes converge with different  $h$  at short time. We will give the additional evidence based on the diffusion results in simulations in the following discussions.

However, for most of the experiments, the lifetime of stickers under the reforming mechanism cannot be easily obtained directly, where the tracing method seems a better characterization.<sup>21,45,46</sup> The key parameters  $\delta$  and  $\zeta$  are essentially the friction coefficients, which will be reflected in the time-dependent MSD in the Fick regime. Different from the linear chains, the dual polymer network cannot move to the Fick regime because of the chemical network restriction, and thus, we put the focus on the relaxation of strands with stickers for simplicity, constructing the relative linear tracer chains. In the MD simulation, we introduce linear chains with the length of  $N = 2n + 1$ , calculating the background friction coefficient  $\zeta$  with the normal tracer and the effective friction coefficient  $\delta$  with the sticky tracer. We introduce five normal tracer chains and five sticky tracer chains without influencing the rheological properties of the matrix. According to the Einstein relation,  $D_{CM}$  is inversely proportional to the friction coefficient acting on the whole tracer. The details can refer to our previous work, here, we only give main points for understanding.<sup>21</sup> To avoid the confusion, we regard  $D_{CM,S}$  as the diffusion coefficient of the tracer chains with stickers and  $D_{CM,N}$  for another, and the effective friction coefficient  $\delta$  can be directly expressed as

$$\delta = (2n + 1) \frac{D_{CM,N}}{D_{CM,S}} - 2n \approx (2n + 1) \frac{D_{CM,N}}{D_{CM,S}} \quad (16)$$

when two diffusion coefficients are equal, meaning stickers and normal beads have the same friction coefficient, and the effective friction coefficient can be calculated as  $\delta = 1$ , which agrees with its definition  $\delta = \zeta_s/\zeta$ . The characteristic time can be determined from the diffusion coefficient, while the Kuhn number must be revised by the characteristic ratio  $C_\infty$ . The corresponding MD simulation results are shown in Figure S6. Diffusion behaviors of the normal tracer are negligible with different binding energies, indicating that the surrounding friction coefficient remains almost the same as the unchanged molecular structure. Based on the deduction above, all parameters can be found in the diffusion motion of tracers. For binding energy  $h$  from 9 to 11, the effective friction coefficients  $\delta$  are supposed to be 63.7, 382.9, and 539, and the background friction coefficient  $\zeta$  is calculated as 34.62, 36.9, and 51.9. Predictions are indicated as solid lines in Figure 9c, where a quantitative agreement exists in these modulus profiles. In the tracing method, we provide only five tracers for avoiding influencing the background friction coefficient. In this case, some tracers may not relax enough at higher  $h$  value, leading to the sample deviation. However, limited by the computing power, the overall number of segments cannot be enlarged, and the deviation exists between MD and tracing predictions, which is roughly consistent without the magnitude error.

Characteristic relaxation time can be calculated using eq 10. Figure 9d shows the predictions of characteristic relaxation time from two methods mentioned above, namely, to obtain the sticker lifetime  $\tau_b$  and the tracer chain diffusion coefficient  $D_{CM,S}$  ( $D_{CM,N}$ ) from MD experiments, and the fitting characteristic relaxation time according to the MD simulations. The one-to-one correspondence strongly suggests that our modified SRM can directly provide an independent prediction of the characteristic relaxation time, which is the key rheological property in practice.

## 5. CONCLUSIONS

In summary, we aim to propose a universal molecular model SRM for predicting dynamic and linear viscoelastic properties of complex associative polymers through constructing permanent and transient dual polymer networks. The idea of the single-chain model for the network and associative polymer is inspired by and based on previous work. Following the single-chain description of permanent networks for studying linear viscoelasticity by Chomppff, Graessley, Kloczkowski et al., we further introduce the idea of effective friction coefficients, which is supposed to be infinite for the peripheral segments anchored to the space. Different friction coefficients can reflect the hindered motion by chemical reactions and the drag force by normal segments. In this way, classic Rouse dynamics can be further extended to the complex dual polymer networks. Section 3 verifies the rationality of the single-chain model for permanent networks, where the supporting results of MD simulations are in well agreement with the prediction of the phantom network at strand length  $N_s = 12$ . For stickers, our previous work has already confirmed that the linear associative polymers can be described using the single-chain model, where the model prediction is consistent with the MD simulations under no fitting parameters. The dual polymer network model provides the whole relaxation mechanism with the analytical solutions of relaxation spectrum, solved by graph theory through simplifying the calculation of the eigenvalues of the sticky RZ matrix. Thus, the analytical expression of the linear

relaxation modulus  $G(t)$  is further obtained, which can return to the case of linear polymers and permanent networks. The analytical results are consistent with experiments, revealing the scale of  $G(t) \propto t^{-1/2}$  for the relaxation of stickers at characteristic time  $\tau_{sb}$ , which becomes an exponential decay beyond its truncation time  $\tau'_{sb}$ .

To establish the universal correlations between the molecular architecture and specific mechanical properties, we study the storage modulus  $G'(\omega)$  and loss modulus  $G''(\omega)$  with frequency and present the effect of intrinsic parameters like effective friction coefficient  $\delta$  and half strand length  $n$ . The sticker characteristic relaxation time  $\tau_{sb}$  becomes larger with increased both  $\delta$  and  $n$ . However, the increase in  $\delta$  leads to the magnified solid elastic characteristics, and the increase in  $n$  strengthens viscous characteristics. The relaxation times estimated from the maximum of loss modulus show well one-to-one correspondence with our analytical results from SRM.

Finally, this work focuses on the prediction role of our modified SRM model for dual polymer networks, where we propose two methods to determine the effective friction coefficient  $\delta$ . In the dual polymer network with measurable lifetime of stickers, the existing time before a sticker finds that new partners can be used for calculating the effective friction coefficient  $\delta$  from our deduced expression in eq 10, showing a perfect agreement with our simulation results of linear relaxation modulus. Another tracing method has more universality for most experiments. The effective friction coefficient  $\delta$  can be extracted from the diffusion coefficient of tracer chains according to the diffusion equation in eq 16, and the quantitative agreement with MD simulations verifies the effectiveness of our SRM model. In conclusion, the present work depicts the physical picture of dual polymer networks and is convenient to predict its dynamics with the SRM at molecular levels, which presents a unified framework for associative polymers.

## ASSOCIATED CONTENT

### Supporting Information

The Supporting Information is available free of charge at <https://pubs.acs.org/doi/10.1021/acs.macromol.1c02059>.

Physical pictures of graph theory for the dual network model, derivation details of analytical eigenvalues and linear relaxation modulus, strand size and MSD simulations for junctions in networks, stress-strain curves, MSDs of tracers, and trapping contribution from entanglements ([PDF](#))

## AUTHOR INFORMATION

### Corresponding Author

Ping Tang – State Key Laboratory of Molecular Engineering of Polymers, Department of Macromolecular Science, Fudan University, Shanghai 200433, China; [orcid.org/0000-0003-0253-1836](https://orcid.org/0000-0003-0253-1836); Email: [pingtang@fudan.edu.cn](mailto:pingtang@fudan.edu.cn)

### Authors

Jingyu Shao – State Key Laboratory of Molecular Engineering of Polymers, Department of Macromolecular Science, Fudan University, Shanghai 200433, China

Nuofei Jiang – State Key Laboratory of Molecular Engineering of Polymers, Department of Macromolecular Science, Fudan University, Shanghai 200433, China

Hongdong Zhang – State Key Laboratory of Molecular Engineering of Polymers, Department of Macromolecular Science, Fudan University, Shanghai 200433, China

Yuliang Yang – State Key Laboratory of Molecular Engineering of Polymers, Department of Macromolecular Science, Fudan University, Shanghai 200433, China

Complete contact information is available at:  
<https://pubs.acs.org/10.1021/acs.macromol.1c02059>

## Notes

The authors declare no competing financial interest.

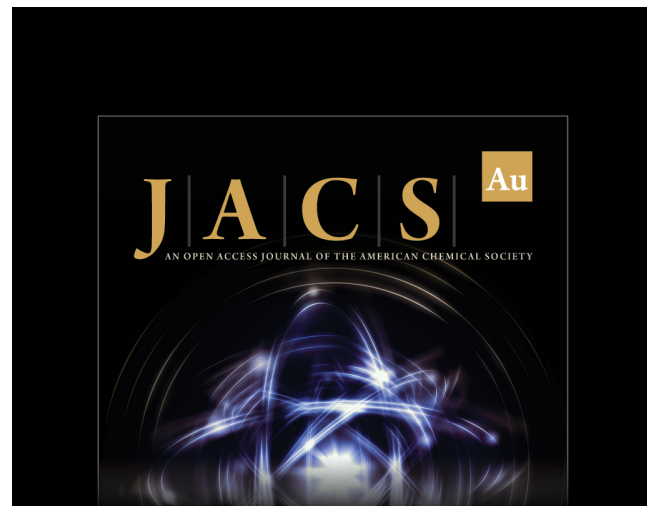
## ACKNOWLEDGMENTS

The authors thank the financial support from the National Natural Science Foundation of China (grant nos. 21774027, 21973017, and 21534002).

## REFERENCES

- (1) Hu, X.; Zhou, J.; Vatankhah-Varnosfaderani, M.; Daniel, W. F. M.; Li, Q.; Zhushma, A. P.; Dobrynin, A. V.; Sheiko, S. S. Programming Temporal Shapeshifting. *Nat. Commun.* **2016**, *7*, 12919.
- (2) Sheiko, S. S.; Dobrynin, A. V. Architectural Code for Rubber Elasticity: From Supersoft to Superfirm Materials. *Macromolecules* **2019**, *52*, 7531–7546.
- (3) Long, R.; Mayumi, K.; Creton, C.; Narita, T.; Hui, C.-Y. Time Dependent Behavior of a Dual Cross-Link Self-Healing Gel: Theory and Experiments. *Macromolecules* **2014**, *47*, 7243–7250.
- (4) Henderson, K. J.; Zhou, T. C.; Otim, K. J.; Shull, K. R. Ionically Cross-Linked Triblock Copolymer Hydrogels with High Strength. *Macromolecules* **2010**, *43*, 6193–6201.
- (5) Hu, X.; Zhou, J.; Daniel, W. F. M.; Vatankhah-Varnoosfaderani, M.; Dobrynin, A. V.; Sheiko, S. S. Dynamics of Dual Networks: Strain Rate and Temperature Effects in Hydrogels with Reversible H-Bonds. *Macromolecules* **2017**, *50*, 652–659.
- (6) Wang, X.; Hong, W. Pseudo-Elasticity of a Double Network Gel. *Soft Matter* **2011**, *7*, 8576.
- (7) Hui, C.-Y.; Long, R. A Constitutive Model for the Large Deformation of a Self-Healing Gel. *Soft Matter* **2012**, *8*, 8209.
- (8) Doi, M.; Edwards, S. F.; Edwards, S. F. *The Theory of Polymer Dynamics*; Clarendon Press, 1988.
- (9) Baxandall, L. G. Dynamics of Reversibly Crosslinked Chains. *Macromolecules* **1989**, *22*, 1982–1988.
- (10) Chomppff, A. J.; Duiser, J. A. Viscoelasticity of Networks Consisting of Crosslinked or Entangled Macromolecules. I. Normal Modes and Mechanical Spectra. *J. Chem. Phys.* **1966**, *45*, 1505–1514.
- (11) Chomppff, A. J.; Prins, W. Viscoelasticity of Networks Consisting of Crosslinked or Entangled Macromolecules. II. Verification of the Theory for Entanglement Networks. *J. Chem. Phys.* **1968**, *48*, 235–243.
- (12) Doi, M. Relaxation Spectra of Nonlinear Polymers. *Polym. J.* **1974**, *6*, 108–120.
- (13) Rubin, R. J.; Zwanzig, R. A Lattice with an Unusual Frequency Spectrum. *J. Math. Phys.* **1961**, *2*, 861–864.
- (14) Graessley, W. W. Elasticity and Chain Dimensions in Gaussian Networks. *Macromolecules* **1975**, *8*, 865–868.
- (15) Graessley, W. W. Statistical Mechanics of Random Coil Networks. *Macromolecules* **1975**, *8*, 186–190.
- (16) Graessley, W. W. Linear Viscoelasticity in Gaussian Networks. *Macromolecules* **1980**, *13*, 372–376.
- (17) Kloczkowski, A.; Mark, J. E.; Erman, B. Chain Dimensions and Fluctuations in Random Elastomeric Networks. I. Phantom Gaussian Networks in the Undeformed State. *Macromolecules* **1989**, *22*, 1423–1432.
- (18) Kloczkowski, A.; Mark, J. E.; Frisch, H. L. The Relaxation Spectrum for Gaussian Networks. *Macromolecules* **1990**, *23*, 3481–3490.

- (19) Kloczkowski, A. Application of Statistical Mechanics to the Analysis of Various Physical Properties of Elastomeric Networks—a Review. *Polymer* **2002**, *43*, 1503–1525.
- (20) Jiang, N.; Zhang, H.; Tang, P.; Yang, Y. Linear Viscoelasticity of Associative Polymers: Sticky Rouse Model and the Role of Bridges. *Macromolecules* **2020**, *53*, 3438–3451.
- (21) Jiang, N.; Zhang, H.; Yang, Y.; Tang, P. Molecular Dynamics Simulation of Associative Polymers: Understanding Linear Viscoelasticity from the Sticky Rouse Model. *J. Rheol.* **2021**, *65*, 527–547.
- (22) Yang, Y. Graph Theory of Viscoelastic and Configurational Properties of Gaussian Chains. *Macromol. Theory Simul.* **1998**, *7*, 521–549.
- (23) Yang, Y.; Qiu, F.; Zhang, H.; Yang, Y. The Rouse Dynamic Properties of Dendritic Chains: A Graph Theoretical Method. *Macromolecules* **2017**, *50*, 4007–4021.
- (24) Yang, Y.; Yu, T. Graph-Theory of Configurational and Viscoelastic Properties of Polymers .2. Linear Polymer-Chains Containing Small Copolymer Blocks. *Macromol. Chem. Phys.* **1986**, *187*, 441–454.
- (25) Kuhn, W.; Grün, F. Statistical Behavior of the Single Chain Molecule and Its Relation to the Statistical Behavior of Assemblies Consisting of Many Chain Molecules. *J. Polym. Sci.* **1946**, *1*, 183–199.
- (26) Wall, F. T.; Flory, P. J. Statistical Thermodynamics of Rubber Elasticity. *J. Chem. Phys.* **1951**, *19*, 1435–1439.
- (27) James, H. M. Statistical Properties of Networks of Flexible Chains. *J. Chem. Phys.* **1947**, *15*, 651–668.
- (28) James, H. M.; Guth, E. Theory of the Elastic Properties of Rubber. *J. Chem. Phys.* **1943**, *11* (10), 455–481.
- (29) Green, M. S.; Tobolsky, A. V. A New Approach to the Theory of Relaxing Polymeric Media. *J. Chem. Phys.* **1946**, *14*, 80–92.
- (30) Chen, Q.; Tudry, G. J.; Colby, R. H. Ionomer Dynamics and the Sticky Rouse Model. *J. Rheol.* **2013**, *57*, 1441–1462.
- (31) Zimm, B. H.; Kilb, R. W. Dynamics of Branched Polymer Molecules in Dilute Solution. *J. Polym. Sci.* **1959**, *37*, 19–42.
- (32) Cai, C.; Chen, Z. Y. Rouse Dynamics of a Dendrimer Model in the  $\theta$  Condition. *Macromolecules* **1997**, *30*, 5104–5117.
- (33) Seiffert, S.; Sprakel, J. Physical Chemistry of Supramolecular Polymer Networks. *Chem. Soc. Rev.* **2012**, *41*, 909–930.
- (34) Everaers, R.; Kremer, K. Topological Interactions in Model Polymer Networks. *Phys. Rev. E: Stat. Phys., Plasmas, Fluids, Relat. Interdiscip. Top.* **1996**, *53*, R37–R40.
- (35) Duering, E. R.; Kremer, K.; Grest, G. S. Structure and Relaxation of End-Linked Polymer Networks. *J. Chem. Phys.* **1994**, *101*, 8169–8192.
- (36) Huang, C.-C.; Xu, H.; Ryckaert, J.-P. Kinetics and Dynamic Properties of Equilibrium Polymers. *J. Chem. Phys.* **2006**, *125*, 094901.
- (37) Hoy, R. S.; Fredrickson, G. H. Thermoreversible Associating Polymer Networks. I. Interplay of Thermodynamics, Chemical Kinetics, and Polymer Physics. *J. Chem. Phys.* **2009**, *131*, 224902.
- (38) Duering, E. R.; Kremer, K.; Grest, G. S. Relaxation of Randomly Cross-Linked Polymer Melts. *Phys. Rev. Lett.* **1991**, *67*, 3531–3534.
- (39) Dossin, L. M.; Graessley, W. W. Rubber Elasticity of Well-Characterized Polybutadiene Networks. *Macromolecules* **1979**, *12*, 123–130.
- (40) Everaers, R.; Sukumaran, S. K.; Grest, G. S.; Svaneborg, C.; Sivasubramanian, A.; Kremer, K. Rheology and Microscopic Topology of Entangled Polymeric Liquids. *Science* **2004**, *303*, 823–826.
- (41) Ramirez, J.; Sukumaran, S. K.; Vorselaars, B.; Likhtman, A. E. Efficient on the Fly Calculation of Time Correlation Functions in Computer Simulations. *J. Chem. Phys.* **2010**, *133*, 154103.
- (42) Schaefer, C.; Laity, P. R.; Holland, C.; McLeish, T. C. B. Silk Protein Solution: A Natural Example of Sticky Reptation. *Macromolecules* **2020**, *53*, 2669–2676.
- (43) Amin, D.; Likhtman, A. E.; Wang, Z. Dynamics in Supramolecular Polymer Networks Formed by Associating Telechelic Chains. *Macromolecules* **2016**, *49*, 7510–7524.
- (44) Stukalin, E. B.; Cai, L.-H.; Kumar, N. A.; Leibler, L.; Rubinstein, M. Self-Healing of Unentangled Polymer Networks with Reversible Bonds. *Macromolecules* **2013**, *46*, 7525–7541.
- (45) Rapp, P. B.; Omar, A. K.; Shen, J. J.; Buck, M. E.; Wang, Z.-G.; Tirrell, D. A. Analysis and Control of Chain Mobility in Protein Hydrogels. *J. Am. Chem. Soc.* **2017**, *139*, 3796–3804.
- (46) Rapp, P. B.; Omar, A. K.; Silverman, B. R.; Wang, Z.-G.; Tirrell, D. A. Mechanisms of Diffusion in Associative Polymer Networks: Evidence for Chain Hopping. *J. Am. Chem. Soc.* **2018**, *140*, 14185–14194.



**JACS Au**  
AN OPEN ACCESS JOURNAL OF THE AMERICAN CHEMICAL SOCIETY

Editor-in-Chief  
**Prof. Christopher W. Jones**  
Georgia Institute of Technology, USA

**Open for Submissions** 

pubs.acs.org/jacsau ACS Publications  
Most Trusted. Most Cited. Most Read.